Analysis of Frequency Locking in Optically Driven MEMS Resonators

Manoj Pandey, Keith Aubin, Maxim Zalalutdinov, Robert B. Reichenbach, *Member, IEEE*, Alan T. Zehnder, Richard H. Rand, and Harold G. Craighead

Abstract—Thin, planar, radio frequency microelectromechanical systems (MEMS) resonators have been shown to self-oscillate in the absence of external forcing when illuminated by a direct current (dc) laser of sufficient amplitude. In the presence of external forcing of sufficient strength and close enough in frequency to that of the unforced oscillation, the device will become frequency locked, or entrained, by the forcing. In other words, it will vibrate at the frequency of the external forcing. Experimental results demonstrating entrainment for a disk-shaped oscillator under optical and mechanical excitation are reviewed. A thermomechanical model of the system is developed and its predictions explored to explain and predict the entrainment phenomenon. The validity of the model is demonstrated by the good agreement between the predicted and experimental results. The model equations could also be used to analyze MEMS limit-cycle oscillators designed to achieve specific performance objectives. **[1499]**

I. INTRODUCTION

ENTRAINMENT is a phenomenon that can occur when a periodic force is applied to a dynamical system whose free oscillation is self-excited, i.e., it vibrates even in the absence of external forcing. If the forcing is strong enough and the frequency difference between the forcing and the unforced oscillation is small enough, the response occurs at a multiple of the forcing frequency rather than at the natural frequency of the system. In such a case, the response is said to be entrained by the forcing function and the system is said to be phase, or frequency locked. A canonical example of entrainment behavior is the Mathieu–Van der Pol oscillator model

$$\ddot{x} + \dot{x}(\alpha + \beta x^2) + (\delta - \epsilon \cos(2t))x = F \cos t \qquad (1)$$

where t is the time and α, β, δ, ϵ, and F are the system parameters. The equation is a combination of two well-known dynamical equations. The first is a Van der Pol equation [1] term $\dot{x}(\alpha + \beta x^2)$, which when $\alpha < 0$ (negative damping for low-amplitude oscillations) leads to steady-state vibrations, called a limit cycle. This limit cycle can be entrained due to the presence of a nonlinear Mathieu equation [1] term $(\delta - \epsilon \cos(2t))x$ or the nonparametric forcing term $F \cos t$, which renders the limit
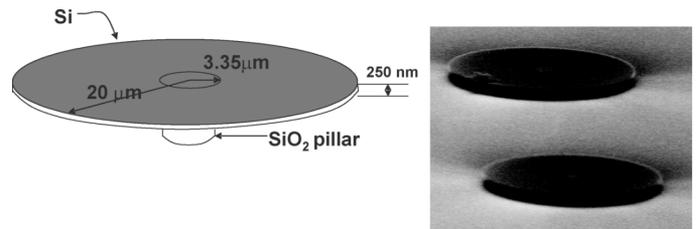
Fig. 1. Disk-shaped oscillator. [Right: scanning electron microscope (SEM) image of actual structure].

cycle unstable in certain regions of the frequency spectrum, allowing it to be entrained [2], [3]. A study of entrainment and the effect of changing the parmeters for 1 is done in [4].

Entrainment in a high Q-factor (10^4), flat-disk-shaped, Si-based, microelectromechanical systems (MEMS) oscillator (Fig. 1) with a tuning range of 50 kHz at a 1.2-MHz operating frequency is described here. An essential feature of this oscillator is that outside of a certain region of the forcing frequency, the device vibrates at a constant amplitude at its natural frequency, independent of the external modulation frequency, while inside the region, the device locks itself to the external modulation. The motivation for such a device comes from the fact that the resonant mode operation of micro and nanoscale oscillators has gained wide interest for applications such as electromechanical filters [5], amplifers, nonlinear mixers [6], [7], atomic scale imaging, scanning probe microscopes, ultrasensitive magnetometers [8], and biological and chemical sensors [9]. Since the resonant frequency of the vibrating sensor carries the information, a fixed resonant frequency limits the applicability of MEMS in many cases. An example is integrated tunable high Q filters which could significantly reduce size and power consumption of telecommunication devices [10], [11]. Similarly, a broadband variable frequency micromechanical oscillator could form the basis of a micromechanical spectrum analyzer. Development of a tunable detector could also greatly benefit magnetic resonance force microscopy (MRFM). Resonant devices can also yield valuable information about the physical properties of materials, especially the sources of internal friction.

In the disk shaped oscillator to be described here, modulation of the absorbed laser energy leads to dynamic thermal stresses that change the stiffness of the device on time scales comparable to the period of vibration [12]. When this occurs, the oscillator is said to be parametrically excited. This term, "parametric excitation," stems from the time varying parameters of the differential equations that describe the motion of an oscillator. In
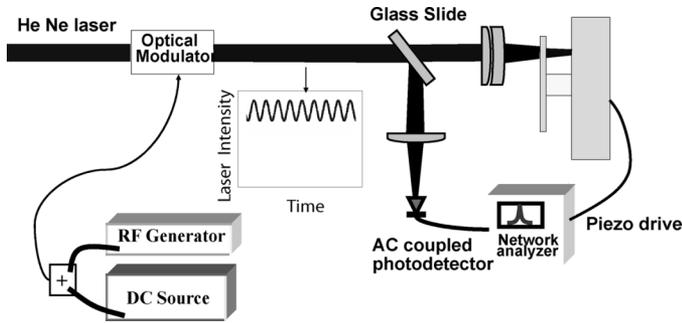
Fig. 2. Experimental setup.

contrast to the case of external excitation, where a small excitation cannot produce a large response unless the drive frequency is nearly resonant, small parametric excitation can produce a large response when the frequency of excitation is at certain integer ratios of the natural frequency of the system. Electrostatically driven parametric resonance in MEMS has been studied by Turner *et al.* [13], [14], Rugar and Grütter [15], and Carr *et al.* [16]. Parametric resonance in an electrostatically driven nanowire was observed by Yu *et al.* [17]. Rugar and Grütter point out that parametric drive can be used not only to amplify motion but to reduce thermomechanical noise as well, greatly increasing sensitivity of sensors built using parametric drive.

Zalalutdinov *et al.* have produced continuous wave (CW) laser driven limit-cycle oscillations in MEMS resonators in the shapes of disks [12], domes [18], paddles [19], and wires. Parametric amplification [20], entrainment [21], and operation in air [19] have been demonstrated. These devices usually are thin (100–250 nm) flexural or torsional structures suspended over a substrate.

Next, we present the experimental setup and results, then the modeling of the system and determination of model parameters, followed by results from the model and predictions of system behavior.

II. EXPERIMENT

A. Setup

The oscillator (Fig. 1) considered here consists of a disk of diameter 40 μm and thickness 250 nm, made of single crystal silicon resting on a SiO_2 pillar of diameter 6.7 μm. The fabrication process is described in [22].

An overview of the experimental setup is shown in Fig. 2. The disk oscillator is placed in a vacuum chamber capable of being pumped to pressures below 1 mtorr, low enough that dissipation due to surrounding gases is insignificant. The samples are situated near a quartz window. A long working distance, 0.35 NA 20 ×, microscope objective is placed outside the vacuum chamber.

Light from a He–Ne laser ($\lambda = 633$ nm) is directed through the microscope objective and focused to a 2-μm diameter spot on the surface of the disk, near its periphery. The incident light is partly transmitted through the thin Si disk. The transmitted component reflects from the substrate back through the disk, interfering with the directly reflected light, forming a Fabry–Perot cavity interferometer. The effect is that the net reflected and ab-

sorbed light intensity are periodic functions of the deflection of the disk at the point of illumination [22]. Thus, the reflected signal, directed into an alternating current (ac)-coupled photodetector, can be used to measure the motion of the oscillator.

The photodetector output is fed into the network analyzer in order to measure and record the amplitude and frequency of the motion. The network analyzer can also output an ac signal of varying amplitude and frequency. This signal is fed to a piezoelectric actuator adhered with double-stick tape to the back of the specimen substrate, providing inertial excitation of the system. The incident laser beam may also be modulated using an RF generator driving an electro-optic modulator.

B. Results

As the direct current (dc) component of the incident laser beam is increased beyond a threshold value, the disk will begin to self-oscillate, i.e., it will vibrate at a resonant mode with a relatively large amplitude of motion, even in the absence of external forcing [23]. The system is said to have undergone a "Hopf bifurcation," wherein a "limit cycle" (oscillation at a single frequency and amplitude) is born out of a "fixed point" (equilibrium position) with a change in one of the system parameters (dc power here). The mechanism for the limit-cycle oscillations is the feedback between deflection of the disk and laser heating. As the disk deflects it moves into a region of higher or lower absorption, changing the temperature of the disk resulting in a thermal driving force. When the thermal driving force is at the correct phase with respect to the motion, (governed by the equilibrium position of the disk with respect to the peaks and valleys of the laser absorption) positive feedback occurs, driving the disk to large oscillations. In addition, temperature changes induce thermal stresses that couple to the bending of the disk, changing its stiffness. The effect is to parametrically drive the system, i.e., drive it by modulation of the spring constant of the oscillator.

With the dc laser intensity set above the threshold for self-oscillation, the disk can be entrained by inertial (piezo) excitation. As the piezodrive frequency f_{pilot} approaches the self-oscillation frequency the motion of the disk is entrained, i.e., the disk begins to vibrate at the piezofrequency (Fig. 3). This case is referred to as 1 : 1 piezopumping. The corresponding amplitude of motion is shown in Fig. 4. The disk vibrates in the symmetric (0,0) mode. The mode was verified by using a second, modulated laser to thermally drive the oscillator about its 1.18-MHz resonant frequency. Scanning the detection laser across the surface of the disk, the phase between the drive and detection lasers was observed to be constant, showing that the mode shape is symmetric.

The amplitude remains at a low, constant value in the region away from the resonance of the structure. This is the amplitude of the limit cycle. The amplitude starts increasing in a region near the resonance of the device. This is called the entrainment region since the disk response is entrained by the driver. Hysteresis of entrainment is seen while sweeping the pilot signal backward.

The total size of the entrainment region (i.e., adding the regions while sweeping forward and backward) is 3.3% of the natural frequency of oscillation. The piezodrive voltage in above
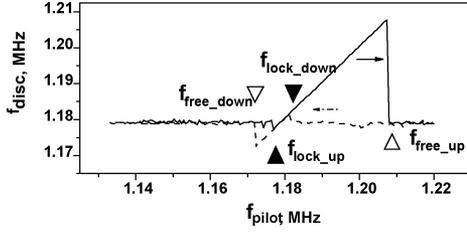
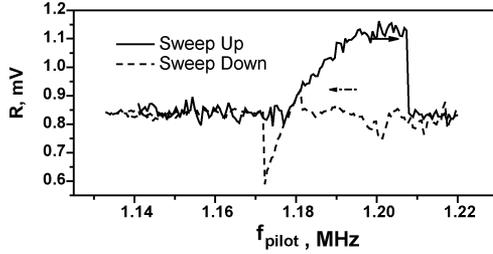Fig. 3. Frequency of response versus piezofrequency, obtained experimentally.

Fig. 4. Amplitude of response versus piezofrequency, obtained experimentally. Amplitude shown as mV output from photodetector. Actual amplitude of motion is shown in [23] to range 80–160 nm or 0.13–0.26 λ.
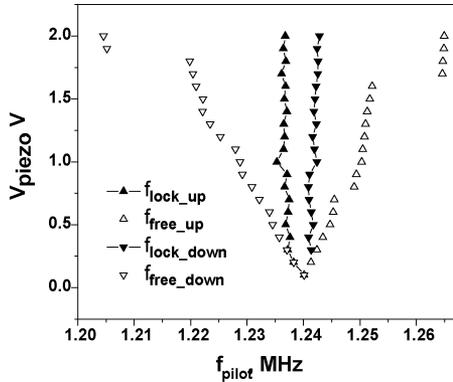

Fig. 5. Entrainment region for varying piezomodulation in $1:1$ piezopumping case, obtained experimentally.

cases was 4 V which roughly corresponds to a base displacement of $0.8 \times 10^{-4} \lambda$, where λ is the wavelength of the incident laser beam. Fig. 5 shows that the entrainment region increases with the amplitude of the inertial modulation.

The disk's motion can also be entrained by modulating the incident laser beam near the frequency ratios of 1 : 1 and 2 : 1 of the disk's limit-cycle frequency, with the piezodrive switched off. The entrainment regions for 2 : 1 laser pumping are shown in Fig. 6, and as before, the entrainment zone increases with the amplitude of the laser modulation.

III. SYSTEM MODEL

A. Model

Although the previously described system is a structure and hence will have spatially varying temperature and deformation fields, it will be simplified for modelling purposes as a 1-DOF nonlinear mass-spring-dashpot system, coupled to the thermal problem through a thermal forcing and a temperature-dependent spring stiffness [12]. Time in the governing equations will be
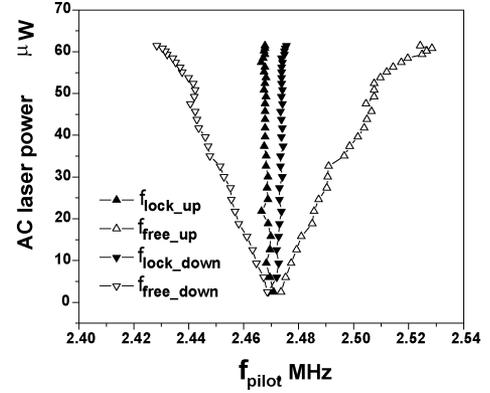

Fig. 6. Entrainment region for varying ac laser modulation in $2:1$ laser pumping case, obtained experimentally.

normalized with respect to the natural frequency of the oscillator and hence the small amplitude frequency is 1.0.

First, consider the thermal model. The rate at which the temperature increases is proportional to the heat input minus the heat loss through the central pillar, which, in accordance with Newton's law of cooling, is proportional to the temperature of the disk. This leads to

$$\dot{T} = AP - BT \qquad (2)$$

where T is the temperature and A and B are thermal constants. The laser power absorbed by the disk is

$$P = P_{\text{laser}}(1 + \varphi \cos(\omega_{\text{laser}}t))(\alpha + \gamma \sin^2(2\pi(z - z_0))) \quad (3)$$

where P_{laser} is the incident laser power, φ is the depth of the laser modulation, and ω_{laser} the frequency of modulation. The $(\alpha + \gamma \sin^2(2\pi(z - z_0)))$ term in (3) approximates the change in the absorbed intensity due to deflection of the disk inside the interference pattern. Here, α is the minimum absorption and γ the contrast. The displacement of the illuminated point of the disk is z and z_0 is the equilibrium position of the disk relative to the laser absorption pattern; both of these quantities are normalized by the λ.

The equation of the vibration of the disk is

$$\ddot{z} + \frac{1}{Q}(\dot{z} - D\dot{T}) + (1 + CT)(z - DT + \beta(z - DT)^3)$$
$$= M \sin(\omega_{\text{piezo}}t) \quad (4)$$

where Q is the quality factor of the oscillator, which is found from the bandwidth of the experimentally obtained amplitude response curve. M represents the amplitude of the sinusoidal base vibration term, which models the external piezodrive. As the temperature increases, radial tensile and hoop compressive stresses are developed that increase the stiffness of vibration modes involving predominantly radial bending and decrease the stiffness of modes involving predominantly hoop bending. The relative stiffness thus is modeled as $(1 + CT)$. C may be positive or negative depending on the structure and mode of vibration. At high frequencies, the temperature modulation away from the point of laser heating diminishes considerably, and thus $|C|$ is a

decreasing function of frequency. The DT term models the optothermal forcing, which arises here from out-of-plane thermal expansion of the disk, which is typically curved due to release of nonuniform residual stresses. This term is treated as a base excitation in (2)–(4). The β term models the structural nonlinearity of this disk.

B. Model Parameters

The parameters of the model [(2)–(4)] are determined using a number of analysis. Using the finite element method (FEM), the transient heat conduction problem of the disk heated over a small region that simulates the laser illumination area is solved. The resulting initial temperature increase rate and steady-state temperature provide the values of A and B, respectively. The temperature field for modulated laser heating is computed as well. The change in stiffness due to the resulting thermal stresses is analyzed by finding the changes in frequency of the (0,0) mode using FEM. Similarly, the cubic stiffness term β and the optothermal drive term D are derived from FEM. Damping Q is estimated from experiments. The optical parameters γ, α, and z_0 are estimated using a film-substrate-gap analysis [24]. The model parameters derived in such a fashion are $A = 0.0176$ °C/μW, $B = 0.488$, $C = 3.53 \times 10^{-4}$/°C, $D = 1.3 \times 10^{-5}$/°C, $\alpha = 0.06$, $\gamma = 0.26$, $M = 0.0001$, $Q = 10^4$, $\beta = 0.375$, and $z_0 = 0.06$. See [25] for more details.

IV. ENTRAINMENT ANALYSIS

The model equations [(2)–(4)] are analyzed using numerical integration. Results of the analysis are compared to the experimental data in order to establish the validity of the model. Fourth-order Runge–Kutta method with adaptive step-sizing is used for integrations. The system is allowed to reach a steady-state [26] at each frequency.

The steady-state results are analyzed to determine the amplitude and frequency of the response. If the frequency spectrum of the response shows a single peak at the forcing frequency, the forcer is said to have entrained the response of the oscillator. In order to simulate the entrainment experiments, in which the frequency is swept, in the numerical experiments the last point of the simulation at the previous frequency is taken as the initial condition for the next step. A step of 0.01 to 0.001 in the normalized frequency is used to compute and plot the amplitude and frequency response against the pilot frequency. From this data, the entrainment region can be determined.

As in the experiments, the disk must first be in a condition of limit-cycle oscillations in order for the motion to be entrained. For the standard parameters, the threshold for self-oscillation is 490 μW, which leads to a steady-state vibration amplitude of $|z| = 0.25$; see [26] for details. The self-oscillations are hysteretic, with the amplitude of motion dropping to zero at 425μW while sweeping P_{laser} backwards.

A. Entrainment Simulations for 2 : 1 Laser Modulation

In the 2 : 1 laser entrainment case, laser modulation is applied at close to twice the natural frequency of the disk oscillator and the response of the system is computed. Fig. 7 shows the calculated dependence of the amplitude of oscillation versus 1/2 the laser modulation frequency.
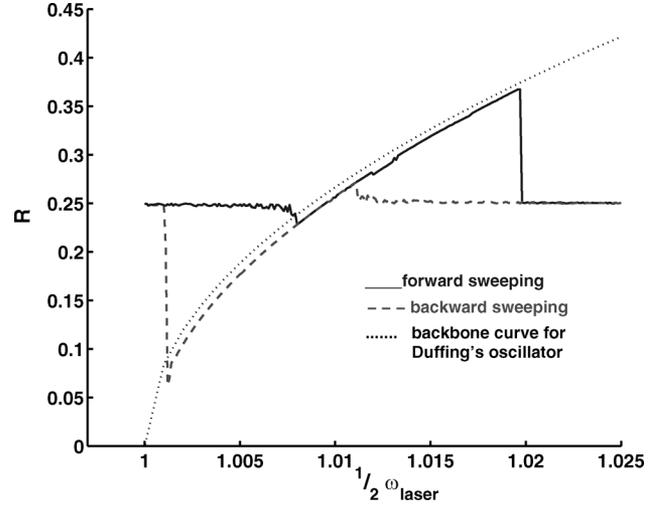
Fig. 7. Amplitude of response R versus 1/2 frequency of laser modulation. $M = 0$, $\varphi = 0.6$, and $P_{\text{laser}} = 600\,\mu$W with 2 : 1 laser modulation, obtained by numerical simulations. Time has been normalized so that the small amplitude frequency is 1.0.

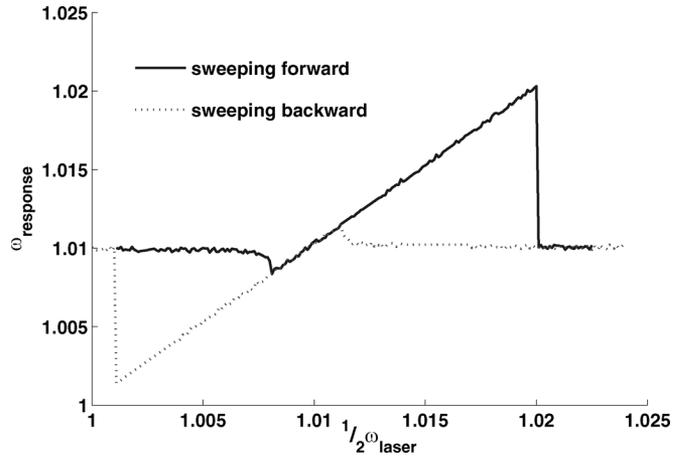Fig. 8. Frequency of the response versus 1/2 frequency of laser modulation. $M = 0$, $\varphi = 0.6$, and $P_{\text{laser}} = 600\,\mu$W with 2 : 1 laser modulation, obtained by numerical simulations. Time has been normalized so that the small amplitude frequency is 1.0.

This simulation is performed for a CW laser power of 600μW and a modulation (φ), of 0.6. Piezodrive is switched off in this case. Away from $\omega = 1$, the amplitude remains constant at around 0.25, the amplitude of the unforced limit cycle. At a frequency of 1.008, the amplitude drops to 0.23 which is the amplitude corresponding to forced oscillation at this frequency. Thus, the forcing function entrains the limit-cycle oscillation at this frequency. After this, the amplitude keeps increasing until a forcing frequency of 1.0198. At this frequency, the amplitude again drops down, when the system loses entrainment. This becomes clearer in Fig. 8 where the response frequency versus 1/2 the frequency of laser modulation is plotted. The frequency of response is almost constant around a value of 1.01, the frequency of the unforced limit-cycle oscillation, and then jumps down to 1.008 at the 1/2 forcing frequency value of 1.008. After this point, the frequency of response is entrained to the forcing frequency and continues to increase until the forcing frequency reaches 1.0198 where it loses entrainment and drops back down
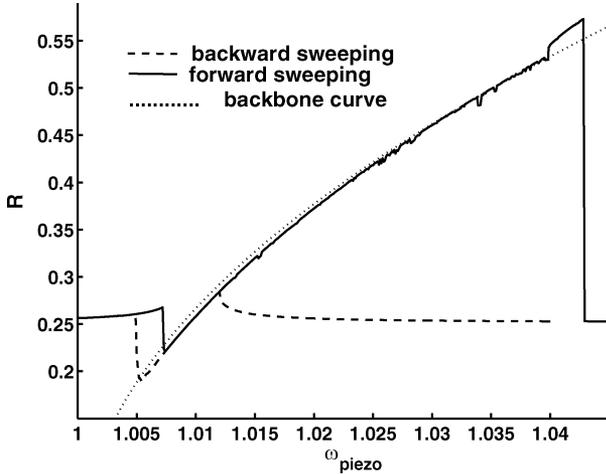
Fig. 9. Amplitude of response R versus frequency of piezodrive, obtained by numerical simulations. $M = 0.0001$, $\varphi = 0.0$, and $P_{\mathrm{laser}} = 600\,\mu\mathrm{W}$ for $1\!:\!1$ piezomodulation.

Fig. 10. Frequency of the response versus frequency of piezodrive, obtained by numerical simulations. $M = 0.0001$, $\varphi = 0.0$, and $P_{\mathrm{laser}} = 600\,\mu\mathrm{W}$ for $1\!:\!1$ piezomodulation.

to 1.01. At frequencies just outside of the entrainment region, beats are observed due to the superposition of the forced response and limit-cycle oscillations.

The bend of the amplitude-frequency curve in the entrainment region is due to the cubic nonlinearity in the system. Plotting the backbone curve, i.e., the curve which gives the relationship between amplitude and frequency for Duffing's equation [1] $(\ddot{z} + z + \beta z^3 = 0)$, gives a good match with the entrainment curve (Fig. 7).

Similar behavior is seen while sweeping the pilot frequency backward. Hysteretic behavior is observed as the entrainment does not occur at the same point as the forward sweep. Initially, the response amplitude remains constant at the limit-cycle amplitude until it reaches the frequency of 1.0111 where it jumps to an amplitude of 0.271 and is entrained. The amplitude reduces as the forcing frequency is decreased until it reaches a value of 1.0012 where entrainment is lost and the amplitude of the response jumps back to the limit-cycle amplitude value.

Thus, from the aforementioned results, we see that in the simulations the entrainment region is 2.2% of the base frequency. Comparing it with the experimental results where the entrainment region is 1.55% shows that the simulations give reasonably good agreement with the experiments.

B. Simulations for 1 : 1 Piezoentrainment

Here we look at simulations for the case when the oscillator is excited using piezodrive close to its natural frequency, while the laser is applied without modulation. The amplitude versus frequency curves for forward and backward sweeping are plotted in Fig. 9.

As before, entrainment occurs over a wide range, from a frequency of 1.0072 to 1.043 while sweeping up and from 1.012 to 1.005 sweeping down. The backbone curve provides a good fit to the entrainment curve.

Similar results are seen in the plot of frequency of response versus frequency of piezodrive (Fig. 10). Comparison with experiments shows good agreement; the total entrainment region is 3.7% for simulation while the experiments showed 3.4% wide entrainment region.
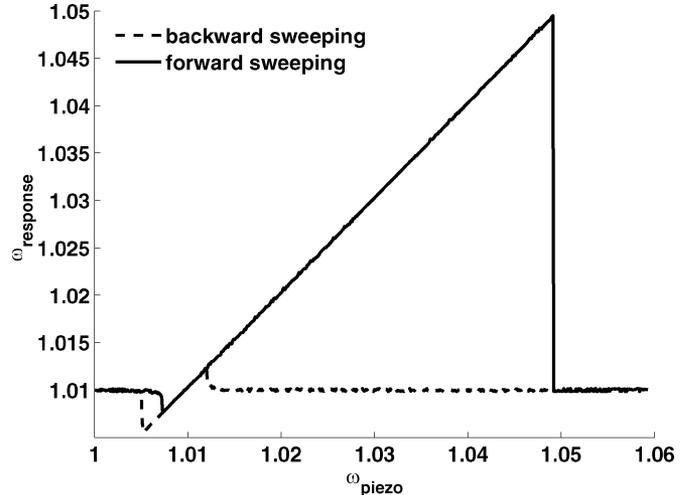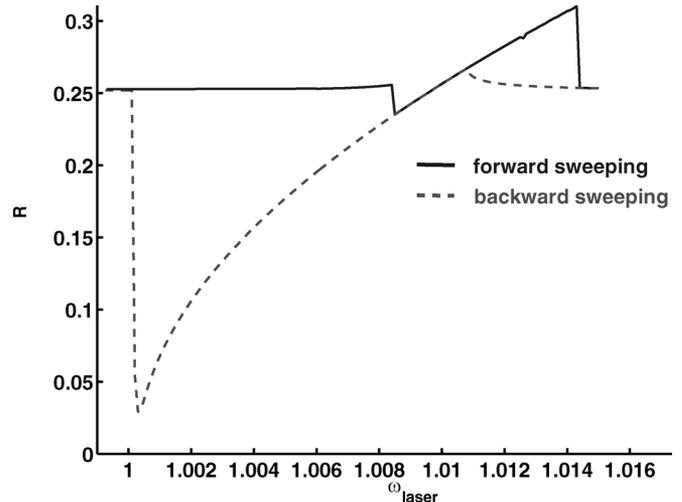

Fig. 11. Amplitude of response versus frequency of laser modulation, obtained by numerical simulations. $M = 0.0$, $\varphi = 0.6$, and $P_{\mathrm{laser}} = 600\,\mu\mathrm{W}$ for $1\!:\!1$ laser-modulation.

C. Simulations for 1 : 1 Laser Entrainment

Simulations for $1\!:\!1$ laser pumping of disk oscillator with the piezodrive switched off are considered next. The amplitude versus frequency plot is shown in Fig. 11. Entrainment is seen in this case while sweeping forward as well as backward. Unlike the previous two cases, the region for entrainment in $1\!:\!1$ laser pumping while sweeping backward is observed to be much larger than the entrainment region in forward sweeping.

D. Effect of Changing Equation Parameters C and D

To study the effects of the parametric term $(1 + CT)$ and the optical drive term (DT) in the model equations, simulations are performed with $C = 0$ and $D = 0$.

First, consider $D = 0$, i.e., the effect of static deflection due to heating is neglected. For $2\!:\!1$ laser modulation case, the system shows entrainment, although the amplitude drops down to zero while sweeping backwards when the entrainment is lost (see
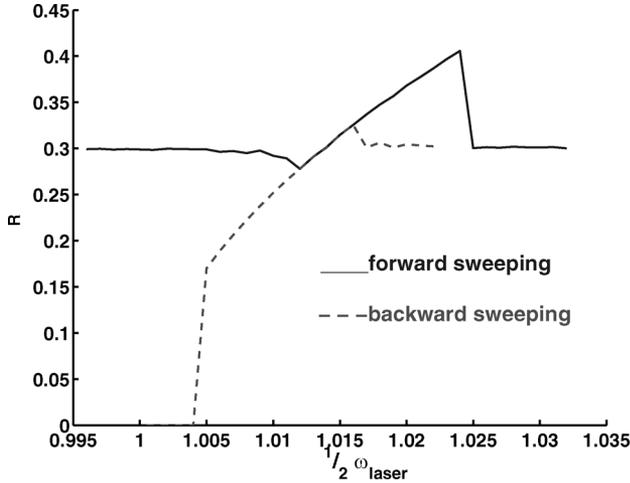
Fig. 12. Amplitude response for $2:1$ laser modulation case , obtained by numerical simulations for $D = 0$, $M = 0.0$, $\varphi = 0.6$, and $P_{\text{laser}} = 920\,\mu\text{W}$ for $2:1$ laser-modulation.

Fig. 14. Amplitude of response versus frequency of piezodrive, obtained by numerical simulations for $C = 0$, $M = 0.0001$, $\varphi = 0.0$, and $P_{\text{laser}} = 600\,\mu\text{W}$ for $1:1$ piezomodulation.
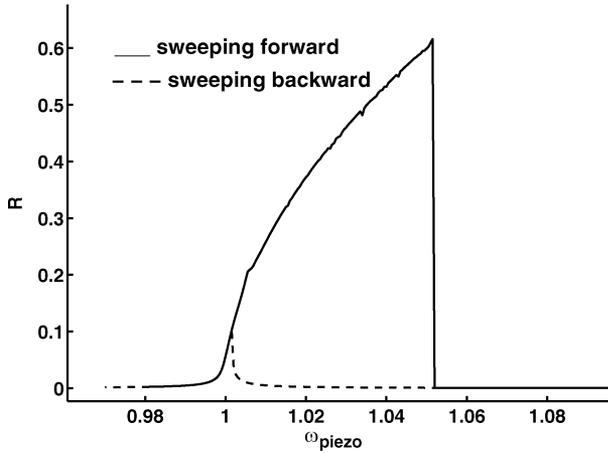

Fig. 13. Amplitude of response versus frequency of piezodrive, obtained by numerical simulations for $D = 0$, $M = 0.0001$, $\varphi = 0.0$, and $P_{\text{laser}} = 600\,\mu\text{W}$ for $1:1$ piezomodulation.

Fig. 12). Entrainment in this case is seen only at a very high value of CW laser power, $920\,\mu\text{W}$ since the Hopf bifurcation threshold increases as D decreases (see [23]). With decreasing D, the Hopf bifurcation changes from subcritical to supercritical. Thus an unstable limit cycle always exists between the stable limit cycle and the equilibrium. If the amplitude during entrainment goes below the unstable limit-cycle amplitude, it will drop to zero when entrainment is lost, instead of jumping back to the stable limit cycle. Hence, the results obtained by neglecting the D term in this case contradict the experimental observations. Note that even at an applied laser power of $1000\mu\text{W}$, the absorbed power is at most $260\,\mu\text{W}$, thus the maximum temperature is $AP/B \approx 10\,^{\circ}\text{C}$ and the change in static deflection due to setting $D = 0$ is $TD \approx 1. \times 10^{-4}\lambda$, an insignificant change that has no impact on the Hopf bifurcation value.

For $1:1$ piezodrive, if $D = 0$, the model predicts that the disk will show the resonant behavior of a forced oscillator (Fig. 13). The limit cycle does not exist and entrainment is not predicted in this case which contradicts the experimental results. The same
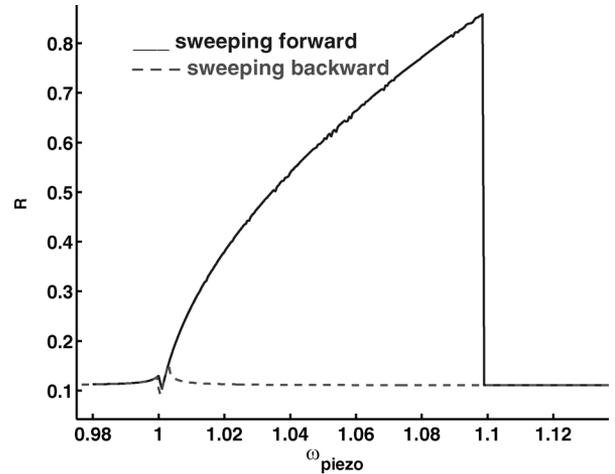
is the case for $1:1$ laser drive. Hence, we see that the optical drive term (DT) is important to model the system correctly.

Next, consider the case when parametric amplification is neglected, i.e., $C = 0$, shown in Fig. 14. In this case the limit cycle occurs, although at a lower amplitude. In $2:1$ laser entrainment simulations, the system never becomes entrained, in contradiction with the experiments.

In the $1:1$ piezocase, for $C = 0$ entrainment is seen between a frequency of 1.001 and 1.098 while sweeping forward and between the frequency of 1.0005 and 1.003 while sweeping backward. The point at which entrainment is lost sweeping backward moves closer to the point where the system is entrained sweeping forward.

In the case of $1:1$ laser pumping case, when $C = 0$, entrainment occurs though the system shows no hysteretic behavior while sweeping backward. Taken together, the results suggest that parametric amplification is needed to accurately model the system.

E. Effect of Changing Strength of Pumping on the Entrainment Regions

In the previous sections, the ac laser modulation was 60% of the CW laser power, i.e., $\varphi = 0.6$. Next, consider the change in entrainment region with φ. Fig. 15 shows two V-shaped regions, each of which represent the entrainment region while sweeping forward and backward in $2:1$ laser entrainment simulations. The point where the system becomes locked is the frequency where the amplitude jumps from the limit-cycle value to the entrained amplitude value. Similarly, the entrainment lost point is the frequency corresponding to the point where there amplitude jumps back to the limit-cycle amplitude. The region of entrainment goes to zero as $\varphi \to 0$ and becomes larger as φ is increased, in accordance with the experimental results (see Fig. 5).

The frequency where entrainment is lost while sweeping backward decreases linearly with ac modulation until $\varphi = 0.5$; it then stabilizes close to 1. On the other hand, the frequency at which the entrainment is lost while sweeping forward keeps
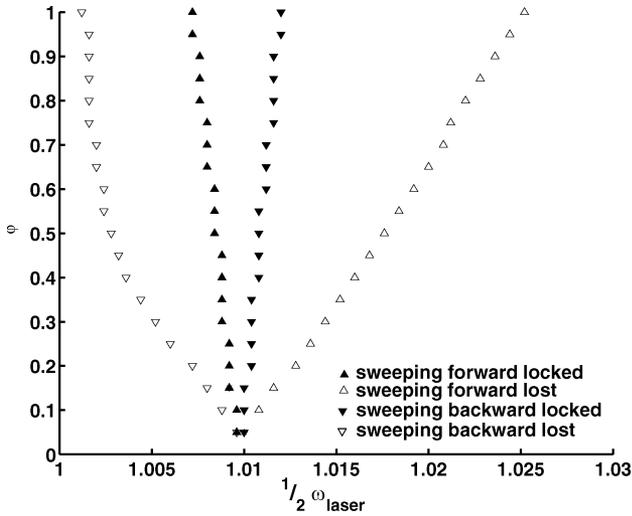
Fig. 15.   Entrainment regions for varying laser modulation, obtained by numerical simulations. $M = 0.0$ and $P_{\text{laser}} = 600\,\mu\text{W}$ for $2:1$ laser-modulation.

Fig. 17.   Entrainment regions for varying power and laser modulation, obtained by numerical simulations. $M = 0.0$ and $P_{\text{laser}} = 450\text{--}750\,\mu\text{W}$ for $2:1$ laser-modulation.
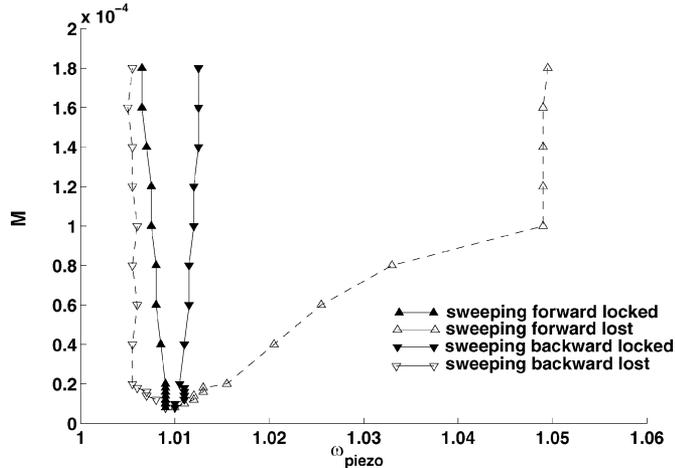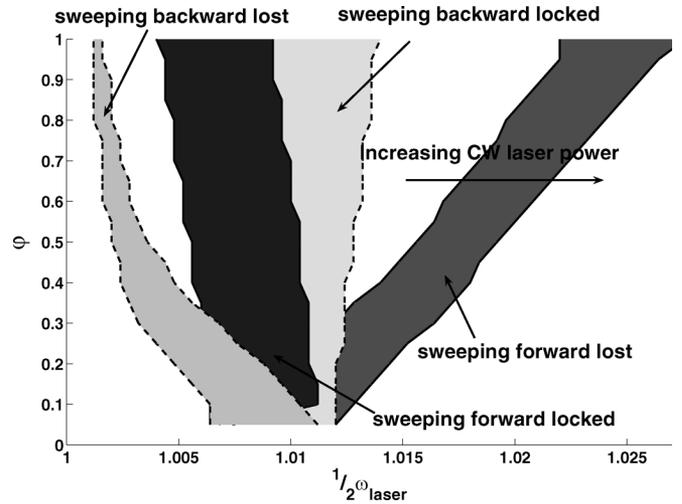

Fig. 16.   Entrainment regions for varying piezoamplitude, obtained by numerical simulations. $\varphi = 0.0$ and $P_{\text{laser}} = 600\,\mu\text{W}$ for $1:1$ piezomodulation.
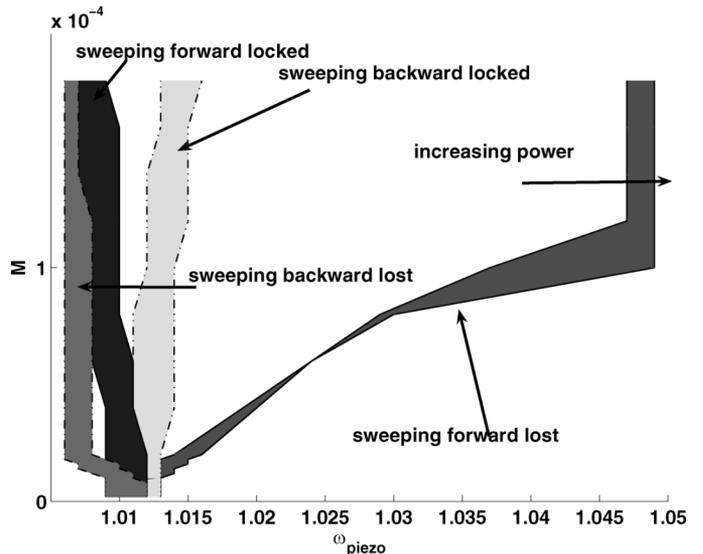

Fig. 18.   Entrainment regions for varying power and piezoamplitude, obtained by numerical simulations. $\varphi = 0.0$ and $P_{\text{laser}} = 6\,600\text{--}750\,\mu\text{W}$ for $1:1$ piezomodulation.

increasing linearly with φ. The total width of the entrainment region increases from zero with $\varphi = 0$ to 2.4% for $\varphi = 1$. The experiments (see Fig. 6) show that for φ varying from 0 to 0.1 the entrainment region increases from 0 to 3.6%.

Similarly, as shown in Fig. 16, the entrainment region for $1:1$ piezopumping increases with increasing amplitude M of the piezodrive. The entrainment region increases with the piezoamplitude, increasing from 0.2% for $M = 1.2 \times 10^{-5}$ to 4.35% for $M = 1.8 \times 10^{-4}$. These results match well with experimentally observed entrainment regions (Fig. 5). Note that the shape of the sweeping forward lost curve in Fig. 16 is somewhat similar to the discontinuity in the $F_{\text{free\_up}}$ curve around 1.7 V in Fig. 5. This experimental behavior was observed consistently.

F. Effect of Changing CW Laser Power on Entrainment Region

Next, consider the effect of changing the CW laser power on the entrainment region. Fig. 17 plots this result as the CW laser power is varied 450–750 μW in the $2:1$ laser entrainment simulations.

The natural frequency of the limit cycle increases, as shown by the rightward movement of the entrainment curves. The total width of the entrainment region increases for increasing laser power from 2% at 500 μW to 2.5% for 750 μW.

In Fig. 18, entrainment regions for $1:1$ piezopumping with varying laser power are plotted. It is seen that the entrainment region shifts right as the CW laser power increases. Thus the base frequency shifts from 1.0095 at 500 μW to 1.013 at 750μW while the maximum width of entrainment changes from 4% to 4.1%.

V. SUMMARY AND CONCLUSION

The disk-shaped device described here will self-oscillate when illuminated by laser light of sufficient intensity. This motion can be entrained, or frequency locked, to a small external

signal. Entrainment by inertial (piezo) drive is demonstrated when the piezo oscillates near a $1:1$ ratio of the self-oscillation frequency. Entrainment by modulating the incident laser at $1:1$ and $2:1$ is also demonstrated.

A mathematical model consisting of a coupled set of mechanical and thermal differential equations is developed to describe the oscillator. The model is analyzed using numerical methods. Numerical integrations show that the model equations predict hysteretic entrainment for $1:1$ inertial, $1:1$ laser, and $2:1$ laser pumping and that as the amplitude of pumping increases, so does the range of entrainment frequencies, all in agreement with the experiments. Numerical experiments show that the parametric term $(1+CT)$ and the direct optical drive term (DT) are both needed in order for the model to agree with experiments.

REFERENCES

[1] A. Nayfeh and D. Mook, *Nonlinear Oscillations*. NY: Wiley, 1979.
[2] G. Litak, G. Spuz-Szpos, K. Szabelski, and J. Warminski, "Vibration analysis of a self-excited system with parametric forcing and nonlinear stiffness," *Int. J. Bifurc. Chaos*, vol. 9, pp. 493–504, 1999.
[3] K. Szabelski and J. Warminski, "Self-excited system vibrations with parametric and external excitations," *J. Sound Vibr.*, vol. 187, pp. 595–607, 1995.
[4] M. Pandey, R. Rand, and A. Zehnder, "Frequency locking in a forced Mathieu-Van der Pol system," presented at the ASME Design Eng. Tech. Conf. (DETC) Long Beach, CA, Sep. 24–28, 2005.
[5] C. T.-C. Nguyen, A.-C. Wong, and H. Ding, "Tunable, switchable, high-Q VHF microelectromechanical bandpass filters," in *IEEE Int. Solid-State Circuits Conf.*, 1999, vol. 448, pp. 78–79.
[6] K. L. Aubin, M. Zalautdinov, R. B. Reichenbach, B. Houston, A. T. Zehnder, J. M. Parpia, and H. G. Craighead, "Laser annealing for high-q MEMS resonators," in *Proc. SPIE*, 2003, vol. 5116, pp. 531–535.
[7] R. B. Reichenbach, M. Zalalutdinov, K. L. Aubin, R. Rand, B. Houston, J. M. Parpia, and H. G. Craighead, "3rd order intermodulation in a micromechanicalthermal mixer," *J. Microelectromech. Syst.*, vol. 14, no. 6, pp. 1244–1252, Dec. 2005.
[8] M. Lohndorf, J. Moreland, P. Kabos, and N. Rizzo, "Microcantilever torque magnetometry of thin magnetic films," *J. Appl. Phys.*, vol. 87, pp. 5995–5997, 2000.
[9] D. Sarid, *Scanning Force Microscopy with Applications to Electric, Magnetic and Atomic Forces*. New York: Oxford Univ. Press, 1994.
[10] C. T.-C. Nguyen, "RF MEMS for wireless applications," in *Proc. 60th Device Res. Conf. (DRC) Conf. Dig.*, 2002, pp. 9–12.
[11] S. Lee, M. U. Demirci, and C.-C. Nguyen, "A 10-mhz micromechanical resonator pierce reference oscillator for communications," in *Proc. 11th Int. Conf. Solid-State Sens. Actuators (Transducers'01), Dig. Tech. Papers*, 2001, pp. 1094–1097.
[12] M. Zalalutdinov, A. T. Zehnder, A. Olkhovets, S. Turner, L. Sekaric, B. Ilic, D. Czaplewski, J. M. Parpia, and H. G. Craighead, "Autoparametric optical drive for micromechanical oscillators," *Appl. Phys. Lett.*, vol. 79, pp. 695–697, 2001.
[13] K. L. Turner, S. A. Miller, P. G. Hartwell, N. C. MacDonald, S. H. Strogatz, and S. Adams, "Five parametric resonances in a microelectromechanical system," *Nature*, vol. 396, pp. 149–152, 1998.
[14] W. Zhang, R. Baskaran, and K. L. Turner, "Effect of cubic nonlinearity on auto-parametrically amplified resonant MEMS mass sensor," *Sens. Actuators A, Phys.*, vol. 102, pp. 139–150, 2002.
[15] D. Rugar and P. Grütter, "Mechanical parametric amplification and thermomechanical noise squeezing," *Phys. Rev. Lett.*, vol. 67, pp. 699–702, 1991.
[16] D. W. Carr, S. Evoy, L. Sekaric, H. G. Craighead, and J. M. Parpia, "Parametric amplification in a torsional microresonator," *Appl. Phys. Lett.*, vol. 77, pp. 1545–1547, 2000.
[17] M.-F. Yu, G. J. Wagner, R. Ruoff, and M. J. Dyer, "Realization of parametric resonance in a nanowire mechanical system with nanomanipulation inside a scanning electron microscope," *Phys. Rev. B, Condens. Matter*, vol. 66, pp. 1–4, 2002.
[18] M. Zalalutdinov, K. Aubin, C. Michael, R. Reichenbach, T. Alan, A. Zehnder, B. Houston, J. Parpia, and H. Craighead, "Shell-type micromechanical oscillator," in *Microtechnologies for the New Millenium*. Bellingham, WA: SPIE, 2003, pp. 5116–5136.
[19] L. Sekaric, M. Zalalutdinov, R. B. Bhiladvala, A. T. Zehnder, J. Parpia, and H. G. Craighead, "Operation of nanomechanical resonant structures in air," *Appl. Phys. Lett.*, vol. 81, pp. 2641–2643, 2002.
[20] M. Zalalutdinov, A. Olkhovets, A. T. Zehnder, B. Ilic, D. Czaplewski, H. G. Craighead, and J. M. Parpia, "Optically pumped parametric amplification for micromechanical oscillators," *Appl. Phys. Lett.*, vol. 78, pp. 3142–3144, 2001.
[21] M. Zalalutdinov, K. Aubin, M. Pandey, A. Zehnder, R. Rand, B. Houston, J. Parpia, and H. Craighead, "Frequency entrainment for micromechanical oscillator," *Appl. Phys. Lett.*, vol. 83, pp. 3281–3283, 2003.
[22] D. W. Carr and H. G. Craighead, "Fabrication of nanoelectromechanical systems in single crystal silicon using silicon on insulator substrates and electron beam lithography," *J. Vac. Sci. Technol., B*, vol. 15, pp. 2760–2763, 1997.
[23] K. Aubin, M. Zalalutdinov, T. Alan, R. Reichenbach, R. Rand, A. Zehnder, J. Parpia, and H. Craighead, "Hopf bifurcation in a disk-shaped nems," in *Proc. 2003 ASME Design Eng. Tech. Conf./19th Biennial Conf. Mech. Vibr. Noise*, Chicago, IL, DETC2003-48516.
[24] Z. Knittl, *Optics of Thin Films*. New York: Wiley, 1976.
[25] K. Aubin, M. Zalalutdinov, R. Rand, A. Zehnder, J. Parpia, and H. Craighead, "Limit cycle oscillations in CW laser driven nems," *J. Microelectromech. Syst.*, vol. 13, no. 6, pp. 1018–1026, Dec. 2004.
[26] M. Pandey, "Entrainment in Disc Shaped MEMS oscillator," M.S. thesis, Cornell University, Ithaca, NY, 2004.

Manoj Pandey received the B.Tech. degree in ocean engineering and naval architecture from Indian Institute of Technology–Madras, Chennai, India, in 2001 and he is currently pursuing the Ph.D. degree in the Department of Theoretical and Applied Mechanics, Cornell University, Ithaca, NY.

His research interest includes the dynamic and finite element analysis of MEMS/NEMS.

Keith Aubin was born and raised in Rhode Island. He received the B.S. degree in physics and mathematics from the University of Rhode Island, Kingston, in 1998 and the Ph.D. degree in applied physics from Cornell University, Ithaca, NY, in 2004.

He is a Postdoctoral Rsearcher at Cornell University working with Prof. Harold Craighead. Before coming to Cornell University, he worked as an Electrical Engineer at Cherry Semiconductor, East Greenwich, RI, and as a Financial Data Analyst in New York. His present research focus is on biological sensors employing nanoelectromechanical systems and microfluidics.

Maxim Zalalutdinov received the Ph.D. degree from the Moscow State University, Moscow, Russia, in 1991.

From 1991 to 1995, he worked with surface analysis and scanning probe microscopy at the Research Institute of Physical Problems, Moscow. From 1995 to 1999, he was with the University of Tokyo, Tokyo, Japan, where his research was related to the physics of quantized vortices in thin super fluid and superconducting films. In 1999, he joined the MEMS group at the Physics Department, Cornell University, Ithaca, NY. His major interest is in nonlinear dynamics of high-frequency MEMS devices.

Robert B. Reichenbach (S'04–M'06) received the B.S. degree in engineering and the B.A. degree in economics from Hope College, Holland, MI, in 2001 and he is currently pursuing the Ph.D. degree in the Department of Electrical and Computer Engineering, Cornell University, Ithaca, NY.

His research interests include the dynamics of NEMS/MEMS resonators and their applications in RF electronics.
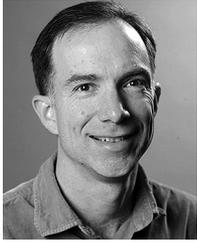
Alan T. Zehnder received the B.S. degree from the University of California, Berkeley, in 1982 and the Ph.D. degree from the California Institute of Technology, Pasadena, in 1987, both in mechanical engineering.

He is a Professor in the Department of Theoretical and Applied Mechanics, the Sibley School of Mechanical and Aerospace Engineering, Cornell University, Ithaca, NY. He has held visiting positions at the Naval Surface Warfare Center, the California Institute of Technology, and the Technical University of Vienna. His research interests are in experimental mechanics, fracture, mechanics of materials, thermomechanical couplings in solids, and the dynamics of NEMS and MEMS.

Harold G. Craighead received the B.S. degree in physics (with high honors) from the University of Maryland, College Park, in 1974 and the Ph.D. degree in physics from Cornell University, Ithaca, NY, in 1980.

He was a Member of Technical Staff and Research Manager, Bell Laboratories and Bellcore. He joined the faculty of Cornell University as a Professor in the School of Applied and Engineering Physics and Director of the National Nanofabrication Facility in 1989. He is currently the Co-Director of the Nanobiotechnology Center. His research focuses on creating nanoscale devices using established and newly developed techniques. The group's projects include studies of single molecule biophysics, chemical sensors, surface patterning for biological and other applications, and the physics of nanoelectromechanical systems (NEMS).

Richard H. Rand received the B.S. degree from Cooper Union, New York, in 1964 and the M.S. and Sc.D. degrees from Columbia University, New York, in 1965 and 1967, respectively, all in civil engineering.

Since 1967, he has been a Professor in the Department of Theoretical and Applied Mechanics, Cornell University, Ithaca, NY. He spent sabbatical leaves in the Departments of Mechanical Engineering at University of California at Berkeley in 1982 and University of California at Los Angeles in 1989. His current research work involves using perturbation methods and bifurcation theory to obtain approximate solutions to differential equations arising from nonlinear dynamics problems in engineering and biology.